DEFENSE TECHNICAL INFORMATION CENTER

Information for the Defense Community

DTIC® has determined on **07 / 16 / 2010** that this Technical Document has the Distribution Statement checked below. The current distribution for this document can be found in the DTIC® Technical Report Database.

☒ DISTRIBUTION STATEMENT A. Approved for public release; distribution is unlimited.

☐ **© COPYRIGHTED**; U.S. Government or Federal Rights License. All other rights and uses except those permitted by copyright law are reserved by the copyright owner.

☐ **DISTRIBUTION STATEMENT B.** Distribution authorized to U.S. Government agencies only (fill in reason) (date of determination). Other requests for this document shall be referred to (insert controlling DoD office)

☐ **DISTRIBUTION STATEMENT C.** Distribution authorized to U.S. Government Agencies and their contractors (fill in reason) (date of determination). Other requests for this document shall be referred to (insert controlling DoD office)

☐ **DISTRIBUTION STATEMENT D.** Distribution authorized to the Department of Defense and U.S. DoD contractors only (fill in reason) (date of determination). Other requests shall be referred to (insert controlling DoD office).

☐ **DISTRIBUTION STATEMENT E.** Distribution authorized to DoD Components only (fill in reason) (date of determination). Other requests shall be referred to (insert controlling DoD office).

☐ **DISTRIBUTION STATEMENT F.** Further dissemination only as directed by (inserting controlling DoD office) (date of determination) or higher DoD authority.

Distribution Statement F is also used when a document does not contain a distribution statement and no distribution statement can be determined.

☐ **DISTRIBUTION STATEMENT X.** Distribution authorized to U.S. Government Agencies and private individuals or enterprises eligible to obtain export-controlled technical data in accordance with DoDD 5230.25; (date of determination). DoD Controlling Office is (insert controlling DoD office).

20100715256

Precision targeting with a
tracking adaptive optics scanning laser ophthalmoscope

Daniel X. Hammer[*a], R. Daniel Ferguson[a], Chad E. Bigelow[a], Nicusor V. Iftimia[a],
Teoman E. Ustun[a], Gary D. Noojin[b], David J. Stolarski[b], Harvey M. Hodnett[b],
Michelle L. Imholte[b], Semih S. Kumru[c], Michelle N. McCall[d],
Cynthia A. Toth[d], Benjamin A. Rockwell[c]

[a]Physical Sciences Inc., 20 New England Business Center, Andover MA 01810;
[b]Northrop Grumman Corporation, 4241 Woodcock Dr, Suite B-100, San Antonio TX 78228-1330;
[c]U. S. Air Force Research Laboratory, 2624 Louis Bauer Dr, Brooks City-Base TX 78235-5128;
[d]Department of Opthalmology, Duke University Medical Center, 127 Erwin Rd, Durham NC 27710

ABSTRACT

Precise targeting of retinal structures including retinal pigment epithelial cells, feeder vessels, ganglion cells, photoreceptors, and other cells important for light transduction may enable earlier disease intervention with laser therapies and advanced methods for vision studies. A novel imaging system based upon scanning laser ophthalmoscopy (SLO) with adaptive optics (AO) and active image stabilization was designed, developed, and tested in humans and animals. An additional port allows delivery of aberration-corrected therapeutic/stimulus laser sources. The system design includes simultaneous presentation of non-AO, wide-field (~40 deg) and AO, high-magnification (1-2 deg) retinal scans easily positioned anywhere on the retina in a drag-and-drop manner. The AO optical design achieves an error of <0.45 waves (at 800 nm) over ±6 deg on the retina. A MEMS-based deformable mirror (Boston Micromachines Inc.) is used for wave-front correction. The third generation retinal tracking system achieves a bandwidth of greater than 1 kHz allowing acquisition of stabilized AO images with an accuracy of ~10 μm. Normal adult human volunteers and animals with previously-placed lesions (cynomolgus monkeys) were tested to optimize the tracking instrumentation and to characterize AO imaging performance. Ultrafast laser pulses were delivered to monkeys to characterize the ability to precisely place lesions and stimulus beams. Other advanced features such as real-time image averaging, automatic high-resolution mosaic generation, and automatic blink detection and tracking re-lock were also tested. The system has the potential to become an important tool to clinicians and researchers for early detection and treatment of retinal diseases.

Keywords: Adaptive optics, scanning laser opthalmoscopy, retinal tracking

1. INTRODUCTION

Adaptive optics (AO) has become increasingly utilized in research ophthalmic diagnostic instruments since their first use nearly ten years ago[1-2]. Recently, Roorda et al. reported the integration of adaptive optics in scanning laser ophthalmoscopy (SLO), a flying-spot technique whereby scattered light in images is blocked by placement of an aperture at a back conjugate focal plane[3]. Adaptive optics systems sense perturbations in the detected wave-front and apply corrections to an optical element that flatten the wave-front and allow near diffraction-limited focus. Much of the aberrations in the eye are static and arise from the cornea and lens but there is also a significant dynamic contribution from the tear film layer. Several groups are working toward moving AOSLO toward clinical use.

The recent progress in the development of AO systems can now begin to be applied toward the major problems that clinicians wish to solve. In general, very high resolution imaging of retinal structures can lead to earlier detection of retinal diseases such as age-related macular degeneration (AMD) and diabetic retinopathy (DR). Combined with other imaging modalities and functional techniques that can explore metabolic ocular health, AO has high diagnostic potential. AO also has the potential to increase our understanding of the fundamental mechanisms of vision and several groups are also working in this area[4].

[*]hammer@psicorp.com; phone 978.738.8224; fax 978.689.3232; psicorp.com

This paper describes our initial investigation in the use AO for the purpose of precision laser targeting. The technology can be applied to studies of vision if the targeting beam is used to stimulate certain retinal structures, such as ganglion cells whose function is yet to be discovered. It can also be used to help study damage mechanisms and determine laser safety thresholds for the use of AO systems. Finally it can be used for precision deliver laser beams for advanced therapies. These therapies could target, for example, RPE cells for selective destruction[5], feeder vessels associated with angiogenesis related to DR, drusen, small tumors, microaneurysms, and epiretinal membranes. Figure 1 shows an illustration of possible precision targeting of RPE cells for the treatment of AMD. There is still disagreement about the effectiveness of this type of treatment to restore vision. It may simply slow the progression of the disease and delay the onset of blindness in elderly, but that is still a worthwhile objective.
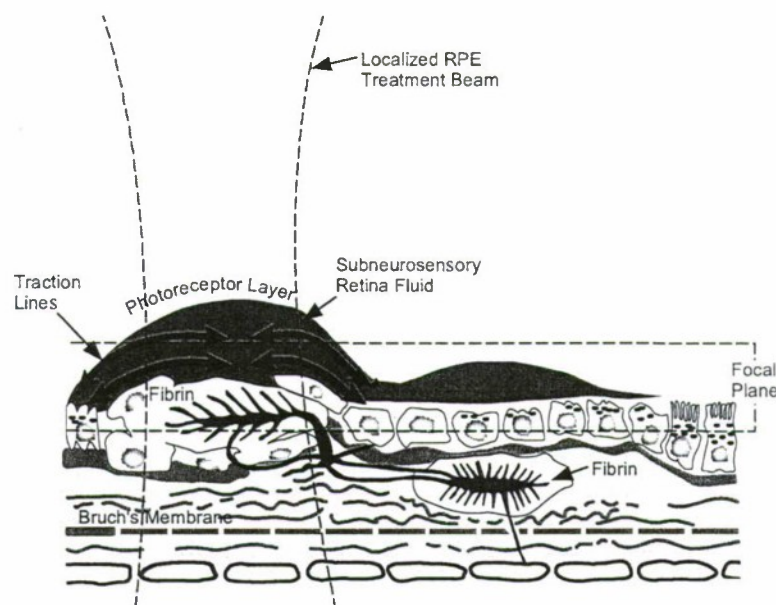

Figure 1: Age-related macular degeneration (AMD) pathology and possible treatment.

We describe a combination of several technologies that may be best suited to the development of an effective, clinical-useful AO system. First, SLO imaging is characterized by high-contrast, confocal en-face retinal views. Second, adaptive optics provides near diffraction-limited and depth-resolved optical access for therapeutic or stimulus beams. Third, retinal tracking mitigates the detrimental effects of eye motion and affords fixed and reproducibly attained retinal coordinates for efficient collection of back-scattered light or delivery of focused beams. Finally, ultrashort pulse damage is characterized by low energy thresholds and spatially-confined disruption because of the non-linear mechanisms that underly it[6]. We have built a system that combines these technologies and this paper reports its first application.

2. MATERIALS AND METHODS

2.1 Overall system architecture

As discussed above, the tracking adaptive optics scanning laser ophthalmoscope (TAOSLO) system used for precision retinal targeting combines scanning laser ophthalmoscopy, adaptive optics, retinal tracking, and ultrashort pulse-mediated tissue disruption. A simplified block diagram of the TAOSLO is shown in Figure 2. A more detailed discussion of the system and retinal tracking performance can be found in another paper in this proceedings[7]. The system uses a dual-imaging approach that simultaneously displays confocal wide-field and high magnification retinal views from the front end TSLO and AOSLO sub-systems, respectively. Thus the position of the AOSLO raster, which often cannot be unambiguously determined from the retinal image information within such a small field, is precisely known, displayed, and controlled by the user. The AO system includes Hartmann-Shack wave-front sensor and deformable mirror wave-front compensator. Diffraction-limited beams are delivered to the eye via a port placed behind the deformable mirror.

Figure 2: Simplified block diagram of TAOSLO system. DM: deformable mirror, HS-WS: Hartmann-Shack wavefront sensor, Dx: dichroic beamsplitter, PBS: pellicle beamsplitter.

2.2 Retinal tracking

The operation of the retinal tracking system has been previously described[8-12]. In this instantiation, the tracking system works with the wide-field line scanning laser opthalmoscope (LSLO)[13] as an independent unit (i.e., the TSLO in Figure 2) but drives two galvanometers placed at appropriate conjugates within the path of the adaptive optics scanning laser ophthalmoscope. The input to the "master" control loop is x-y error signals generated from the track beam dithered on a feature and detected from a confocal reflectometer. The input to the "slave" control loop is the scaled position signals from the master galvanometers. The slave tracking mirrors are placed at conjugates to the center of rotation of the eye. This allows line-of-sight tracking (i.e., simultaneous tracking of the pupil and retina from rotational eye motion) because the mirrors pivot about the true axis of rotation of the eye. Besides the dual-imaging advantage, this master-slave configuration of the retinal tracker as integrated into the AOSLO has advantages of minimal impact on the AOSLO optical train, standard configuration and implementation of both the AOSLO and retinal tracker optics and electronics, AOSLO image stabilization on targets over the wider LSLO field (40-deg compared to <15-deg), and potential advanced tracking schemes such as adaptive error-signal filtering and head (i.e., translational) motion tracking. This configuration does require a one-time calibration between master and slave systems. Moreover, the tracking accuracy can suffer if there is a significant disparity between the position of the track target and the AOSLO raster because of geometric considerations and torsional eye motion. This is often the case since the optic nerve head (the bright reflection from the lamina cribrosa) is our primary tracking feature and the macular region is our primary imaging target.

Our retinal tracking system has recently been upgraded. We have re-configured the system so that all tracking functions are performed by a single set of stacked electronics boards. Future engineering will reduce the tracking electronics to a single small printed circuit board. Communication between the tracking boards and host computer is accomplished via a USB interface. Control parameters are passed to and reflectance, position, and error signals are received from the tracking board. The blink detection and track re-lock algorithm was refined but generally operates in a manner similar to previous systems[12]. The control and processing electronics include a field programmable gated array (FPGA) chip that performs digital lock-in amplification and other pre-processing steps, a digital signal processor (DSP) that performs two proportional-integral-derivative (PID) control loops (for master and slave systems), and analog-to-digital and digital-to-analog converters (ADC and DACs) to receive reflectometer signals and drive galvanometers. The DSP has a loop rate of 62.5 kHz (compared to 16 kHz in the previously-used real-time processing board) for a closed loop bandwidth well in excess of 1 kHz. The tracking beam wavelength was shifted from the 800-900-nm range used in previous systems to 1060 nm to accommodate typical superluminescent diodes (SLD) used in SLO and optical coherence tomography (OCT) systems. The other major tracking hardware upgrade (shifting the resonant scanner – and dither frequency – up to 16 kHz from 8 kHz) has yet to be implemented in this system [12].

2.3 Optics

The AOSLO component of the system is arranged in a typical manner. The SLO flying-spot raster is accomplished with a 12-kHz resonant scanner in the fast x-axis and a galvanometer in the slow y-axis. These mirrors are placed at papillary

conjugates to pivot the retinal scan from a stationary beam at the pupil. The entire resonant scanner is attached to a galvanometer. This configuration, where offsets can be applied to galvanometers along both axes of the raster, allows advanced scans to be created (e.g., 4-5-deg macular montage pieced together automatically from single SLO frames). A near-infrared source (830-nm LD or 800-nm SLD with 30-nm bandwidth, Exalos Inc.) is used for SLO illumination and an avalanche photodiode detector (Hamamatsu Inc.) with confocal pinhole (100 and 200-μm diameter) is used for detection. The AO system uses a Hartmann-Shack wave-front sensor (HS-WS) comprised of a 65×65-element lenslet array (0.4-mm pitch and 25-mm focal length, Adaptive Optics Associates Inc.) and a 1024×1024-pixel CCD camera with a maximum frame rate of 60 Hz and camera-link interface (Dalsa Inc.). Wavefront sensing is done with a 670-nm AO beacon. The beacon is placed in front of the deformable mirror (DM) to minimize distortion from mirror surface irregularities and to de-couple mirror-induced wavefront errors during mirror-sensor calibration. It is placed behind the scanning mirrors to provide smoother spots and improve the accuracy of the centroid algorithm[14]. A 141-element MEMS-based, continuous-surface, electrostatic-actuator-driven DM (Boston Micromachines Inc.) is used for wave-front correction. The DM has a diameter of only 4.8-mm so long paths are not required to magnify the pupil.

The optics were designed to de-magnify a 6-mm pupil through the small resonant scanner mirror, to fill the DM (to use all actuators) and magnify again to nearly fill the WS camera. Spherical mirrors are primarily used to limit back-reflections, minimize chromatic distortion, and, since the system will be used to deliver short pulses to the eye, minimize dispersive pulse broadening. One drawback is that spherical mirrors used off-axis will induce astigmatism in the beam. We have developed a novel and complex three-dimensional optical arrangement that uses spherical mirrors in an arrangement that minimizes astigmatism. Focus adjust of up to 10 diopters is achieved with two stages: one on which the entire system is placed that controls the space between a front lens relay (custom designed in Zemax to minimize spherical and chromatic aberrations and control field flatness), and a second smaller stage that adjusts the position of the DM within the system. TSLO focus is adjusted independent of the AOSLO focus. The AOSLO optical design achieves an error of <0.45 waves (at 800 nm) over ±6 deg on the retina including front lens relay.

The LSLO source for wide-field imaging is a 905-nm SLD. The combined power of the four wavelengths that enter the eye – 670, 830, 905, and 1060-nm for the AO beacon, SLO beam, LSLO beam, and tracking beam – always remained below ANSI standard thresholds. Typical powers used were 35, 300, 200, and 100 μW, respectively.

2.4 Electronics and instrumentation
In addition to the tracking electronics described briefly above, the instrumentation for the system includes 3 framegrabbers (analog for SLO, digital camera-link for WS, and digital for LSLO), custom camera and timing boards, digital timing boards to control the DM, and a 8×8 LED array for fixation controlled via the serial port. The custom timing board provides a non-linear pixel clock to the analog framegrabber to automatically linearize the sinusoidal scan produced by the resonant scanner. This board also provides vertical and horizontal sync signals to the framegrabber, to the SLO LD/SLD for modulation, and to the "Exsync" signal of the WS camera-link framegrabber. The modulation creates a blanking region for the analog framegrabber. A physical mask placed in the optical train cannot be used to create a blanking region while the retinal tracker operates because the raster is moved about the field as the eye moves. Synchronization between the SLO and WS frames assures congruency between each WS slope and the retinal coordinate of the corrected AOSLO image. This means that wave-front correction is insensitive to errors from a lack of eye isoplanicity, although this contribution to wave-front distortion is small and we have also run the cameras asynchronous. The LSLO and SLO systems are not synchronized since they use optical paths entirely independent of one another. The LSLO camera acquires a 512×512-pixel frame at 15 frames/sec. The 12-kHz resonant frequency of the SLO scanner enables a 512×512-pixel frame rate up to ~25 frames/sec. In practice, we operate at half that speed since the images from all three components (LSLO, SLO, and WS) are acquired and displayed by a single software platform.

In addition to acquisition, display, and processing of the three images, the software controls communication with the tracking board, WS spot position and slope calculation, AO (WS/DM) calibration, AO closed-loop operation, wave aberration and Zernicke coefficient calculation and display, and logging of tracking signals, AVI videos (from all three cameras), and single images in a variety of formats. When a live video was streamed to disk, two additional files were saved that contained track data (reflectance, x-y track mirror positions, and either the x-y error signals or the x-y slave mirror positions) in binary format and a text file that contained all system parameters and calibration factors.

For AO-correction using the continuous-surface DM, a one-time calibration is performed subsequent to system alignment to find the influence of each actuator on its neighbors and to establish a baseline for calculation of slopes. The software uses a standard algorithm for spot centroid determination that operates at the frame rate of the WS camera up to 30 Hz. During AO-correction, the local wave-front slopes are found and inverted with a pseudo-influence function and fed to the DM driver. The wave aberration function and Zernicke coefficients can be calculated in real-time, though this is not usually done during measurement to preserve processor resources for more critical functions. The closed-loop bandwidth of the AO system is ~2-3 Hz. Streaming videos requires processing and often slightly reduces the frame rate further.

2.5 Human and animal subject test plan

The system was tested to characterize AO-corrected imaging and tracking performance in human volunteers. Prior to examination, informed consent was obtained from all volunteers. Depending upon the experiment, the data acquired included wide-field LSLO images, wave-front slopes (from which the Zernicke coefficients, wave aberration function and point spread function can be calculated), videos and track data with and without retinal tracking, videos with and without adaptive compensation (at best focus), videos to compare AOSLO imaging source, and macular montages. Several of those experiments are discussed in another paper in this proceedings[7].

Preliminary tests on cynomolgus monkeys was also performed at Brooks City-Base TX in August 2005 to investigate the feasibility of and determine the effect of delivery of aberration-corrected ultrashort pulse beams to the retina for various studies and applications related to damage mechanisms, laser safety, and precision targeting for advanced therapies and vision studies. A photograph of the setup taken during the experiments at Brooks is shown in Figure 3. For these tests, the system was configured to accept an additional visible laser beam through a port placed behind the DM and scanners. This port can also be configured to deliver other types of stimulus sources for other applications. A solid-state titanium:sapphire laser system was configured to deliver short pulses to the eye. The wavelength and pulse duration of the ultrashort pulses were 150 fs and 532 nm, respectively. Although we sought to maintain a power at the cornea of $10\times$ the minimum visible lesion threshold of 160 nJ, the maximum power we could achieve at the cornea was roughly $5\text{-}10\times$ the threshold, up to several μJ. There was only 10-20% broadening of the short pulses through the TAOSLO system – almost entirely from the front lens relay.
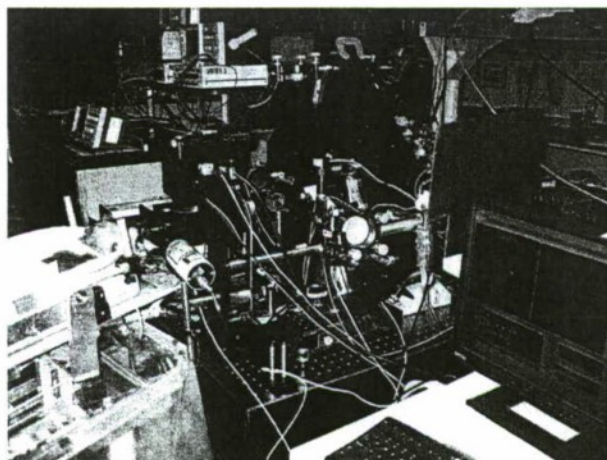

Figure 3: Photograph of the TAOSLO system during testing at Brooks City-Base in August 2005.

Lesions were delivered at precise retinal coordinates within the raster field by synchronization of the laser trigger with the SLO raster. The ability to place multiple lesions was limited by the low repetition rate of the laser used in this study since only one lesion could be placed during one SLO frame and multiple lesions require multiple frames – a possibility only enabled by retinal tracking. Future studies with other higher repetition rate laser sources may allow line and patch lesions or stimuli to be delivered to the retina.

The monkeys were maintained and prepared according to normal humane practices governed by federal regulations [15]. Details of the standard animal preparation can be found elsewhere[16]. The experiments planned on monkeys included imaging and lesion creation with and without adaptive compensation, imaging and targeting of retinal layers through-depth (nerve fiber layer to choriocapillaris), patch and line lesions, and other advanced scanning methods. Since the monkeys were anesthetized with peribulbar injections that immobilized the eye, retinal tracking was not required. Subsequent to imaging and lesion delivery, the eyes were enucleated and retinal tissue fixed. The lesions are currently being stained, sectioned, and examined with microscopy at Duke University.

3. RESULTS

3.1 Imaging performance of AOSLO system

The TAOSLO system was designed and characterized with Zemax optical design software prior to construction. The aim of the optical design was to minimize inherent system aberrations across the SLO field of view to reserve as much deformable mirror stroke as possible for correction of ocular aberrations. Figure 4 shows the results of the AOSLO design on-axis. At the edge of the field of view, the maximum wave-front error was 0.44 waves but was <0.25 waves for much of the 12-deg field of view.
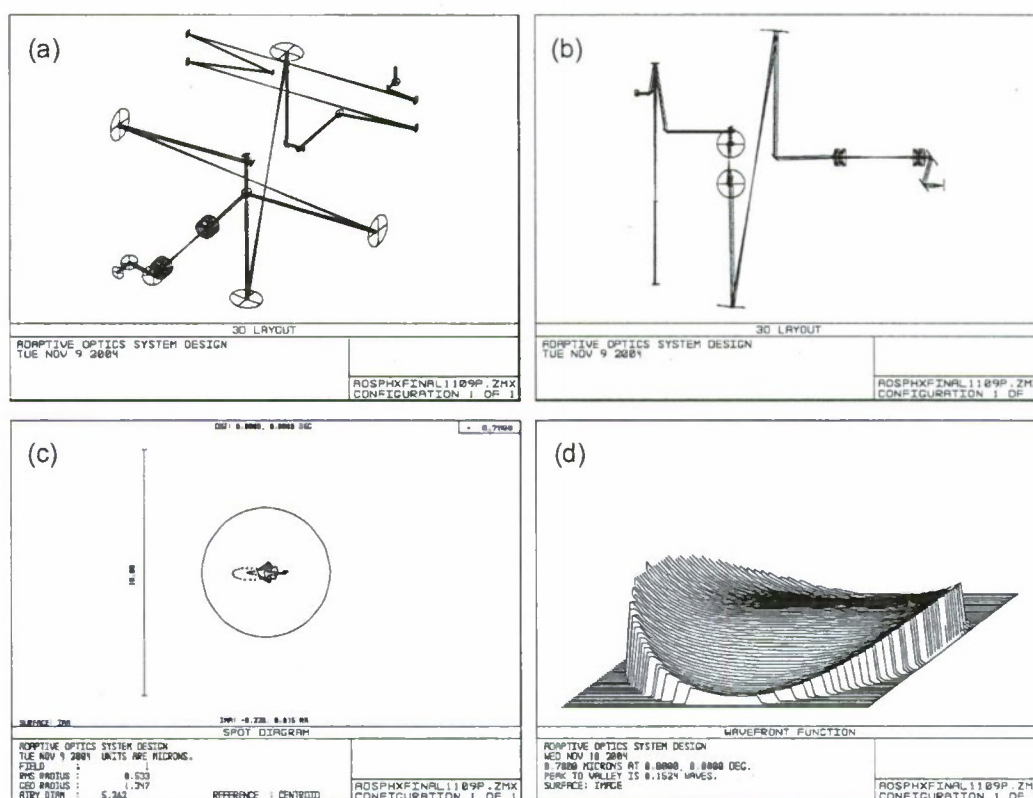
Figure 4: TAOSLO designed optical performance on-axis. (a-b) two views of the optical layout, (c) spot diagram, and (d) wavefront error.

Although we did not dilate the eyes of the human subjects tested and therefore only expected limited AO correction with 3-5-mm pupils (the eye has nearly optimal point spread function for pupils ~2-3 mm in diameter[17]), we were able to realize significant improvement in the SLO images with adaptive compensation of ocular aberrations. In part this was due to the careful optical design and alignment prior to system characterization but also to the excellent ocular optics of the young healthy subject initially tested. We were able to resolve the cone mosaic in all individuals (5 men, 1 woman,

mean age = 36), but it was especially clear in the youngest subjects. While aberrations are often characterized and corrected to 10-orders of Zernicke polynomials, de-focus and other lower-order aberrations are usually the dominant reason for poor SLO image quality. Our acquisition software has a slider to adjust to the optimum focus during AO correction. This, in addition to the manual stages described above, provided fine control over focus. We observed qualitatively that the AO correction often drove the focus to deeper retinal layers. To illustrate the true improvement in appearance, resolution, and contrast, we acquired two images in identical retinal regions while adjusting the system for best focus. The result is shown in Figure 5. Without AO correction (Figure 5a), the cones are clearly resolved in most areas but their appearance is significantly degraded compared to the case with AO correction (Figure 5b). The mean±standard deviation of the histogram is 42.5±25.8 without correction compared to 75.3±44.2. The comparison of histograms shows improved contrast in the AO image as measured by standard deviation.
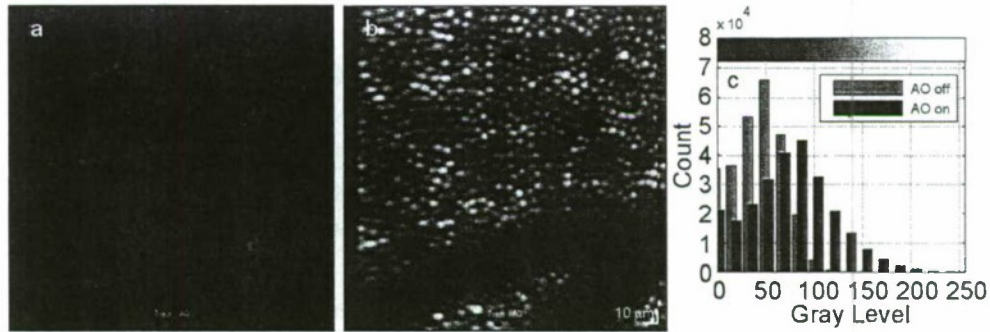
Figure 5: Best focus of AOSLO imaging system (a) without and (b) with adaptive optics correction and (c) comparison of histograms from (a) and (b).

We also examined the effect of source coherence on image quality. Because the SLO is an imaging system with a confocal aperture and intrinsic sectioning capability, it is subject to the pernicious effect of speckle noise. This noise arises from the coherent superposition of light reflected from scatterers within the coherence length of the source. For a source with a long coherence length, speckle noise reduces resolution and contrast while shorter coherence length sources yield images with less corruption from multiple scattering. Figure 6 shows images acquired from the same retinal region using a superluminescent diode with 30-nm bandwidth (Figures. 6a and b) compared to a laser diode (Figures 6c and d) with and without AO correction.
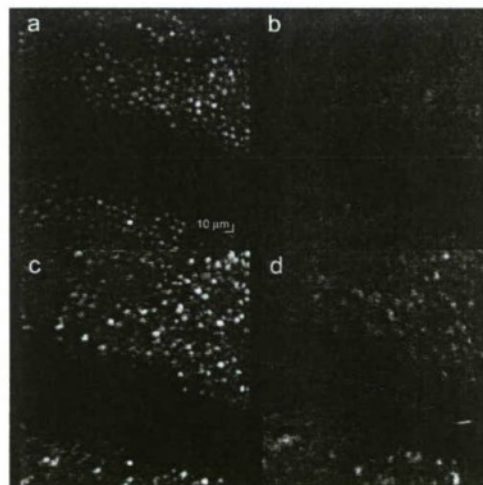

Figure 6: Comparison of high coherence and low coherence imaging sources for AO. (a) low coherence superluminescent diode with AO, (b) same without AO, (c) high coherence laser diode with AO, (d) same without AO.

3.2 Results of animal tests

Many of the system refinements discussed herein were implemented subsequent to the experiments at Brooks City-Base. For example, all AOSLO images collected at Brooks used a laser diode for illumination. Moreover, an earlier generation deformable mirror with lower stroke (2 μm vs. 3.5 μm) was used, the SLO raster was set up for a larger field (~2 deg), and the LSLO camera was not properly configured. This, combined with the inherent difficulty of experiments with animals and ultrashort pulse laser systems alike, made the investigation all the more arduous. Despite these challenges, we were able to deliver AO-corrected beams to the animals, although the cone mosaic was not resolved. We did not attempt to deliver lesions to different layers, but we did image through the depth of a large marker lesion produced with a millisecond pulse Argon ion laser. We did not deliver patch or line lesions for the reasons discussed above. Ocular aberrations were measured on each eye and color fundus photographs were collected at 1 and 24 hour intervals after lesion placement.

Lesions were produced with and without AO correction in four eyes of two cynomolgus monkeys. Two of the eyes contained previously placed lesions in the macula and so new lesions were placed extra-macular. The minimum visible lesion threshold roughly doubles in this region compared to the macula[18]. We have yet to verify if the initial development of any lesion was resolved in the AOSLO videos. Histology will reveal whether the AO-corrected lesions are more confined in either transverse or axial spatial extent compared to the lesions produced without AO correction.

In general, the ocular aberrations were slightly larger in monkeys than humans. Since the eyes of the animals were kept open with a speculum and moistened with saline drip every ~5-10 seconds during the experiment, one concern is corneal drying. We measured the ocular aberrations of one monkey at the end of the day three times consecutively between saline drips to determine the variability over a time roughly equivalent to the imaging and laser delivery time between drips. Figure 7 shows the results. The top panel shows the wave aberration function for the three trials and their mean and standard deviation on equivalent gray scales and the bottom panel plots 7-orders of Zernicke coefficients on three plots with different scales. The coefficients show ~20-30% variability, which is approximately what one would expect between blinks from the tear film layer in humans.
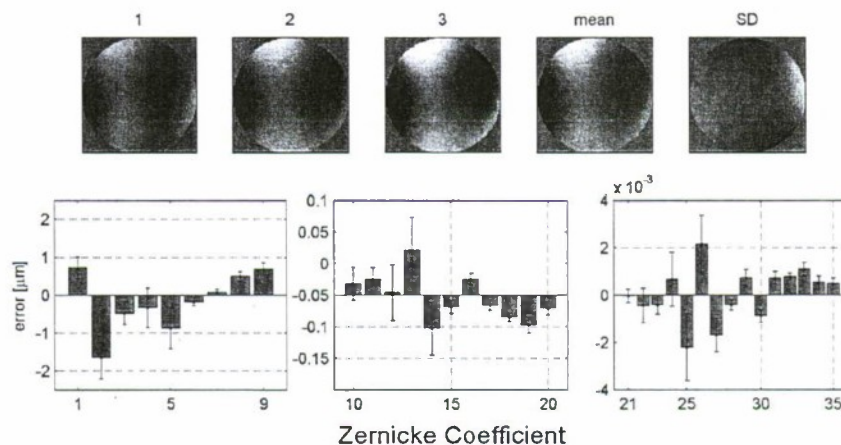

Figure 7: Ocular aberration measurement on a cynomolgus monkey. Top row: wave aberrations for three consecutive measurement and their mean and standard deviation. Pupil diameter = 6 mm. Bottom row: Zernicke coefficients (mean ± SD) for the wave aberrations. Note the change in y-scale in the three plots.

3.3 Results of human subject tests

The primary objective of the initial human subject investigation reported herein was characterization of the performance of retinal tracking and adaptive optics components. A secondary goal was to test the operation of several advanced AOSLO scanning modes enabled by retinal tracking, such as real-time averaging and automated montage acquisition. Unlike in previous OCT and SLO systems, the AOSLO system has the transverse resolution necessary to measure tracking accuracy with the necessary precision. The master-slave configuration worked well and except for rapid saccades, there was little discrepancy between master and slave mirror positions. Excluding those rapid saccades, the RMS tracking accuracy was between 5 and 15 μm for all subjects tested. The blink/track re-lock software also worked

well and was able to re-lock after most blinks during longer scans. The performance of the tracker and some strategies for advanced tracking methodologies specifically suited to adaptive optics is discussed in another paper in this proceedings[7]. Future publications will highlight the advanced AOSLO scanning modes.

To characterize AO performance in eyes absent disease or other structures of interest, we were primarily concerned with resolving cone mosaic although we also imaged erythrocytes in retinal vessels and the capillary network. Figure 8 illustrates SLO images obtained from a young, healthy volunteer with and without AO correction. As discussed above, the best AO correction occurred when initially focused (prior to turning AO on) more superficially in the retinal vasculature (Figure 8b). The cone mosaic is clear in the corrected image. The cone mosaic was resolved but not as sharply as in equivalent images acquired from older subjects (>35 years). Most of this is due to the fact that undilated eyes were imaged and future studies using mydriatic agents may yield optimal results for all subjects.
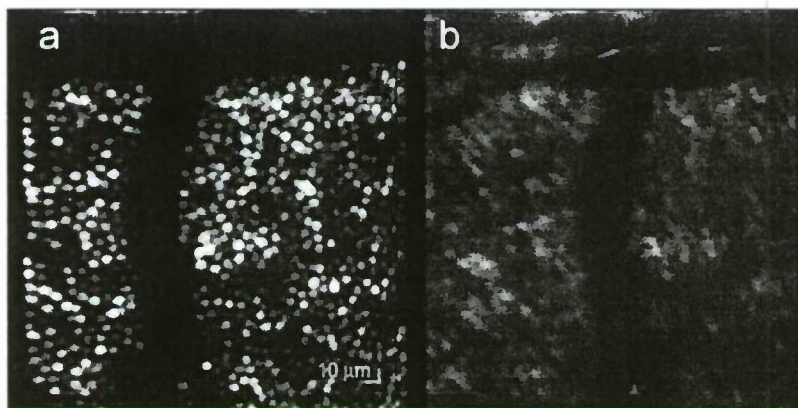

Figure 8: Images of cone mosaic acquired from a young, healthy volunteer (a) with and (b) without adaptive optics correction.

4. DISCUSSION

We have designed, built, and characterized in animals and humans an adaptive optics scanning laser ophthalmoscope with active retinal stabilization. The system uses a novel optical arrangement, integrated software platform, and advanced electronics and instrumentation for the generation of high resolution, aberration-corrected, stabilized scans of the retina. The system was easily configured to acquire advanced scans such as macular montages. We tested the effect of source bandwidth and found substantial improvement with the use of superluminescent diodes. Although this may add slightly to the eventual cost of a clinical system, the benefits far outweigh the cost. The retinal tracking system uses a master-slave configuration and further strategies will pursue scalable precision to the level of a single cone. Even for the best fixators, without retinal tracking eye motion can slew the field of regard to non-overlapping retinal locations reducing useable frames and image correspondence for longer duration scans and longitudinal studies. In a clinical scenario that includes predominantly elderly patients with limited ability to fixate, retinal tracking may prove invaluable for small AO fields. We demonstrated a significant improvement in the visualization of the retina with retinal tracking. We resolved the cone mosaic in all subjects tested. Although the system was not yet optimized at the time of the animal experiments, histology may show lesions confined in both transverse and axial dimensions.

The TAOSLO system can be used for a wide variety of applications, from the selective destruction of diseased cells during the progression of retinal diseases, to a finer probing of the visual system, to the examination of lesion development and further understanding of the mechanisms of retinal disruption. We will pursue these and other applications in future work.

ACKNOWLEDGEMENTS

REFERENCES

1. J. Liang, D. R. Williams, and D. Miller, "Supernormal vision and high-resolution retinal imaging through adaptive optics," J. Opt. Soc. Am. A **14**, 2884-2892,1997.
2. A. Roorda and D. R. Williams, "The arrangement of the three cone classes in the living human eye," Nature, **397**, 520-522 , 1999.
3. A. Roorda, F. Romero-Borja, W. J. Donnelly III, H. Queener, T. J. Hebert, and M. C. W. Campbell, "Adaptive optics scanning laser ophthalmoscopy," Opt. Express, **10**, 405-412, 2002.
4. Heidi Hofer, Joseph Carroll, Jay Neitz, Maureen Neitz, and David R. Williams, "Organization of the Human Trichromatic Cone Mosaic," J. Neuroscience, **25**, 9669-9679, 2005.
5. C. Alt, C. Framme, S. Schnell, H. Lee, R. Brinkman, and C. P. Lin, "Selective targeting of retinal pigment epithelium using an acousto-optic laser scanner," J. Biomed. Optics, **10**, 064014, 2005.
6. C. A. Toth, D. G. Narayan, C. P. Cain, G. D. Noojin, K. P. Winter, B. A. Rockwell, and W. P. Roach, "Pathology of macular lesions from subnanosecond pulses to visible laser energy," Invest. Opthalmol. Vis. Sci. **38**, 2204-2213, 1997.
7. R. D. Ferguson, D. X. Hammer, C. E. Bigelow, N. V. Iftimia, T. E. Ustun, S. A. Burns, A. E. Elsner, and D. R. Williams, "Tracking adaptive optics scanning laser ophthalmoscope," paper 6138-36, in Ophthalmic Technologies XVI, Eds: Manns, Soderberg, and Ho.
8. D. X. Hammer, R. D. Ferguson, J. C. Magill, M. A. White, A. E. Elsner, and R. H. Webb, "Image stabilization for scanning laser ophthalmoscopy," *Opt. Express* **10,** 1542-1549, 2002, http://www.opticsexpress.org/abstract.cfm?URI=OPEX-10-26-1542.
9. D. X. Hammer, R. D. Ferguson, J. C. Magill, M. A. White, A. E. Elsner, and R. H. Webb, "Compact scanning laser ophthalmoscope with high speed retinal tracker," *Appl. Opt.* **42**, 4621-4632, 2003.
10. R. D. Ferguson, D. X. Hammer, L. A. Paunescu, S. Beaton, and J. S. Schuman, "Tracking Optical Coherence Tomography," *Opt. Lett.*, **29**, 2139-2141, 2004.
11. D. X. Hammer, R. D. Ferguson, J. C. Magill, L. A. Paunescu, S. Beaton, H. Ishikawa, G. Wollstein, and J. S. Schuman, "An Active Retinal Tracker for Clinical Optical Coherence Tomography Systems," *J. Biomed. Opt.*, **10**, 024038, 2005.
12. D. X. Hammer, R. D. Ferguson, N. V. Iftimia, T. E. Ustun, G. Wollstein, H. Ishikawa, M. L. Gabriele, W. D. Dilworth, L. Kagemann, and J. S. Schuman, "Advanced scanning methods with tracking optical coherence tomography," *Opt. Express*, **13**, 7937-7947, 2005, http://www.opticsexpress.org/abstract.cfm?URI=OPEX-13-20-7937.
13. D. X. Hammer, R. D. Ferguson, T. E. Ustun, C. E. Bigelow, N. V. Iftimia, R. H. Webb, "Line-scanning laser ophthalmoscope," *J. Biomed. Opt. (Special Issue for A. J. Welch)*, in press.
14. H. Hofer, P. Artal, B. Singer, J. L. Aragón, and D. R. Williams, "Dynamics of the eye's wave aberration," J. Opt. Soc. Am. A., **18**, 497, 2001.
15. The animals involved in this study were procured, maintained, and used in accordance with the Federal Animal Welfare Act and the "Guide for the Care and Use of Laboratory Animals" prepared by the Institute of Laboratory Animal Resources – National Research Council. Brooks City-Base TX has been fully accredited by the Association for Assessment and Accreditation of Laboratory Animal Care, International (AAALAC) since 1967.
16. C. P. Cain et al., "Thresholds for visible lesions in the primate eye produced by ultrashort near-infrared laser pulses," Investigative Ophthalmology and Visual Science, **40**, 2343-2349, 1999.
17. E. J. Fernández and W. Drexler, "Influence of ocular chromatic aberration and pupil size on transverse resolution in ophthalmic adaptive optics optical coherence tomography," Opt. Express **13**, 8184-8197, 2005, http://www.opticsinfobase.org/abstract.cfm?URI=oe-13-20-8184.
18. C. P. Cain et al., "Comparison of macular versus paramacular retinal sensitivity to femtoscond laser pulses," J. Biomed. Optics, **5**, 315-320, 2000.